



# Solution-processed nanostructured ZnO/CuO composite films and improvement its physical properties by lustrous transition metal silver doping

A. Akkaya<sup>1</sup> · B. Şahin<sup>2</sup> · R. Aydın<sup>3</sup> · H. Çetin<sup>4</sup> · E. Ayyıldız<sup>5</sup>

Received: 13 May 2020 / Accepted: 12 July 2020 / Published online: 23 July 2020  
© Springer Science+Business Media, LLC, part of Springer Nature 2020

## Abstract

This paper has reported the fabrication and characterization of pristine, and silver (Ag)-doped nanostructured ZnO/CuO composite thin films that have not been previously reported. The thin films were synthesized by the successive ionic layer adsorption and reaction (SILAR) technique. The morphological, crystalline structure, optical and electrical characterizations of the films have been achieved utilizing scanning electron microscopy (SEM), energy-dispersive spectrometry (EDS), atomic force microscopy (AFM), X-ray diffraction (XRD) analysis, Fourier transform infrared spectrum (FTIR) analysis, ultraviolet–visible (UV–Vis) spectrophotometry and the four-point probe measurements. Particle sizes of pristine and Ag-doped ZnO/CuO thin films were found to vary from 32 to 58 nm. Crystallite size was changed from 16.40 to 18.90 nm with changing Ag dopant in the ZnO/CuO composite film. FTIR spectra that have the absorption peaks at  $\sim 725$  and  $\sim 510$   $\text{cm}^{-1}$  referred to the stretching vibration of Zn–O and Cu–O bonds during the synthesis of ZnO/CuO nanofilms. The bandgap values of ZnO/CuO composite films increased from 2.05 to 2.36 eV as Ag content increased from 0 to 2 M%. The activation energies of the samples were obtained from the Arrhenius plots of  $\sigma$  versus  $1/T$ . The multiple activation process was observed. It was noteworthy that Ag-doping results in a significant difference in conductivity at all temperature values.

## 1 Introduction

Nowadays, many researchers focus on the synthesis and examination of composite multicomponent nanostructured metal-oxide materials. Nanostructured metal-oxide based heterostructures are more prepossessing because of the easy availability, non-toxic character, likelihood of integrating the main chemical and physical properties and chemical and

biological stability [1, 2]. Diverse nanostructured composite materials have been presented, including Graphene/ZnO [3],  $\text{TiO}_2/\text{CdS}$  [4], ZnO/CuO [5], ZnO/CdO [6],  $\text{SnO}_2/\text{ZnO}$  [7], ZnO/ $\text{Co}_3\text{O}_4$  [8], ZnO/ $\text{Fe}_2\text{O}_3$  [9], NiO/ZnO [10], and  $\text{Gd}_2\text{ZnMnO}_6/\text{ZnO}$  [11].

Among these nanostructured composite materials, ZnO/CuO thin films much attractive owing to their unique and superior properties such as environmental friendly and low price [12]. Zinc oxide (ZnO) is a II–VI compound and an n-type semiconductor with a wide bandgap of about 3.4 eV. Additionally, ZnO is a metal oxide with high exciton binding energy of 60 meV at room temperature and hexagonal wurtzite crystal structure. Also, ZnO has unique attributes like high thermal and chemical stabilities, perfect substrate devotion, not containing poisonous substances, semiconductor features with doping and abundance in nature [13, 14]. Meanwhile, nanocomposite ZnO has attracted attention due to its optical properties. It has been presented that ZnO could absorb photons with energy higher than the optical bandgap energy of metal-oxide semiconductor and execute hole and electrons [15, 16]. Copper oxide (CuO) is a p-type semiconductor having a narrow energy gap of about 1.5 eV [17, 18]. CuO is also a nontoxic, inexpensive contains

✉ A. Akkaya  
abdullah.akkaya@ahievran.edu.tr

<sup>1</sup> Mucur Technical Vocational Schools, Tech.Prog.  
Department, Ahi Evran University, Kırşehir, Turkey

<sup>2</sup> Laboratory of Nanostructured Materials and Applications,  
Faculty of Arts and Sciences, Mustafa Kemal University,  
Antakya, Hatay, Turkey

<sup>3</sup> Department of Physics, Faculty of Sciences, Selçuk  
University, Konya, Turkey

<sup>4</sup> Department of Physics, Faculty of Arts and Sciences, Bozok  
University, Yozgat, Turkey

<sup>5</sup> Department of Physics, Faculty of Sciences, Erciyes  
University, Kayseri, Turkey

exceptional morphologic versatility, chemically stable and abundant material [19]. Therefore, heterostructures of these two metal-oxides into a structure could be an influential way to adjustment of main physical properties, such as solar cell, sensor, optoelectronic device, photocatalysis and antibacterial activity efficiencies [11, 20, 21].

Doping is one of the potent ways to improve the primary physical and chemical properties of nanostructured metal oxide composite films. The physical characteristics of composite films can be enhanced by adding various elements such as Mn [22], Ce [23], La [24], Er [25] and Ag [26] to the films. Amongst different doping elements, Ag is preferable as a dopant source because Ag has high metal reflectivity, the highest electrical conductivity of  $6.3 \times 10^7$  S/m, and perfect thermal conductivity [27, 28]. The impact of Ag dopant material on the thin film features have been investigated by some researchers [29, 30]. The nature of silver ions is simple link matrices. Thus, doping of Ag in ZnO/CuO nanocomposite could result in varied structural and morphological properties and hence could affect its physical performance. Surface morphological and crystalline structural modifications were made to enable these materials as efficient optoelectronic devices.

It is significant to examine the system of multicomponent nanostructured metal-oxide, such as how the optoelectronic properties and electrical conductivity are modified when the composition varies. Hence, this research aimed to work out the main physical properties of the nanostructured ZnO/CuO composite films and the contingency of implementations in electronically and optoelectronic materials.

As far as we know, there has been no recorded research where silver-doping on nanostructured ZnO/CuO composite samples were researched for their surface morphological, structural, optical, and electrical properties. We have used the SILAR technique to growth pristine and silver doped ZnO/CuO composite films. It has been reported that doping of silver ions vigorously impresses the main physical properties of nanostructured ZnO/CuO composite thin films.

## 2 Experimental procedure

### 2.1 Synthesis of nanostructured ZnO/CuO composite thin films

In this research, nanostructured ZnO/CuO composite thin films were grown by the SILAR method on silica glass substrates at room conditions. To prepare the film growth solution, analytical zinc acetate dihydrate and copper(II) chloride dehydrate reagents were used. 2.19 g zinc acetate dehydrate (Formula:  $\text{Zn}(\text{CH}_3\text{COO})_2 \cdot 2\text{H}_2\text{O}$ , Molecular Weight: 219.51 g/mol and Assay: 99.9%) and 1.70 copper(II) chloride dehydrate (Formula:  $\text{CuCl}_2 \cdot 2\text{H}_2\text{O}$ ,

Molecular Weight: 170.48 g/mol and Assay: 99%) were weighted and mixed with 200 ml double distilled water to obtain 0.1 M zinc acetate and 0.1 M copper(II) chloride solution respectively. Then they were mixed at room condition for 5 min for the obtain a transparent and well-dissolved solution. Double distilled water and ammonium hydroxide ( $\text{NH}_4\text{OH}$ ) were used as solvents. After stirring, the pH value of the growth solution was then increased to  $10.0 \pm 0.02$  by adding  $\text{NH}_4\text{OH}$  while the solution was heated up and kept at  $85^\circ\text{C}$ . Soda-lime glass substrates were precleaned using three steps which were cleaning in dilute sulfuric acid solution ( $\text{H}_2\text{SO}_4:\text{H}_2\text{O}$ , 1:5 by volume), in acetone, and in double-distilled water for 10 min, each in an ultrasonic bath. The substrates were rinsed in the mixed growth solution for 20 s and then into the deionized hot water ( $85^\circ\text{C}$ ) for 20 s to remove loosely bound species from the substrate. This process was repeated for 25 times to obtain nanostructured ZnO/CuO composite thin film. Figure 1 presents the schematic diagram of SILAR method for deposition of nanostructured ZnO/CuO composite thin films.

To examine the effect of varying percentages of silver (Ag) as a dopant on ZnO/CuO composite thin films, three series of (the ratio of Ag are 0%, 1 M%, and 2 M%, respectively) samples were produced. Silver nitrate (Formula:  $\text{AgNO}_3$ , Molecular Weight: 169.873 g/mol and Assay: 99%) was used as source precursors for Ag. The reaction bath for the first one was pristine solution (i.e. contains only zinc acetate, copper(II) chloride, water and ammonia), the sechend baths were containing 1 and 2.0 M% (Molar percent) Ag ions, respectively. Then, pristine and silver-doped nanostructured ZnO/CuO composite thin films were annealed at 523 K ( $250^\circ\text{C}$ ) for 45 min. in a PROTHERM PTF 12/50/450 tube furnace in air ambient.

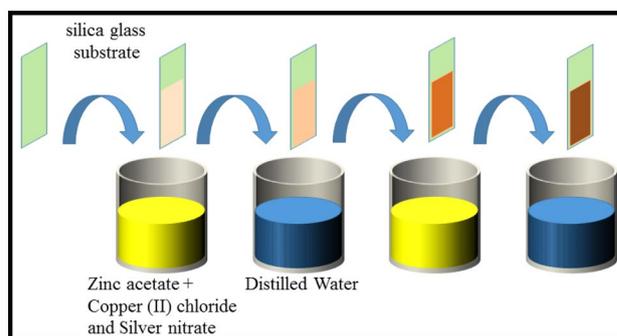


**Fig. 1** The schematic diagram of SILAR method for deposition of nanostructured ZnO/CuO composite thin films

## 2.2 Characterizations of nanostructured ZnO/CuO composite thin films

The surface morphology of samples was observed using the FE-SEM (The Zeiss SUPRA 55-VP) with EDS and AFM (Solaris Atomic Force Microscope). XRD patterns were recorded by Bruker D8 advance high-resolution diffractometer (Cu K $\alpha$  radiation,  $\lambda = 1.540056 \text{ \AA}$ ). The thickness of samples was measured via Nanomap - 500LS 3D Surface Profilometer. The optical absorbance and transmittance properties of samples were examined by Thermo Scientific Genesys 10 s UV-Vis. Spectrophotometer in the 400–1100 nm wavelength range. The presence of chemical bonding in nanostructured ZnO/CuO composite thin films was studied by Thermo Scientific Nicolet 6700 FTIR spectrometer in the range of 4000–400  $\text{cm}^{-1}$  with a resolution of 1  $\text{cm}^{-1}$ .

The four-point probe measurements were used to obtain resistivity values. The measurements were performed with a software equipped probe station in which distance between probe centers of the axis is 1.5 mm. All the measurements were taken in a stainless steel vacuum chamber to avoid samples react with the atmospheric gases. The chamber was equipped with feedthrough to ensure electrical connection, and its pressure was kept at  $2.5 \times 10^{-3}$  mTorr during the measurements. The measurements were performed in the range of  $1 \times 10^{-6}$ – $1 \times 10^{-4}$  A constant current with  $1 \times 10^{-6}$  A steps to reach more accuracy. The software of the measurement system, which includes a statistical analysis program, reported that all the measurement quality was high.

The resistivity of samples were measured in the range of 293–403 °K in a vacuum chamber. Lakeshore 332 S was used to control substrate heating and a calibrated diode fixed onto the samples to measure the temperature.

## 3 Results and discussions

### 3.1 Surface morphological studies of nanostructured ZnO/CuO composite thin films

Surface morphological features of the thin films have remarkable importance on their main physical features. Such as, a change in particle size, distribution or surface roughness result a difference in electronic properties of materials. In order to be intensified the influence of the doping methodology on morphology at both the micro and nanoscale, in this research, two microscopic methods, SEM and AFM have been used.

The SEM images of the ZnO/CuO composite films are shown in Fig. 2. From the SEM images, it can be understand that all the substrates are fully covered by ZnO/

CuO nanocomposite, and all images show dense surfaces. According to Fig. 2, nearly homogeneous particle deployment has been expressly seen, and the almost smooth surface has also been observed. After the doping of silver, the particle sizes changing about between 32 and 58 nm and smoothly distributed are executed on the surface. Similar homogeneous distributed SEM results have been observed by other researchers [31, 32]. Since main physical properties of the nanostructured metal-oxide structures are dependent to particle size and morphology of them, it is significant to be able to prepare the product with a controlled structure, particle size and distribution [33].

Figure 3 presents extended SEM pictures of pristine and 2 M% silver-doped ZnO/CuO composite films. The average particle sizes of the samples have been predicted from the images. The estimated values of the particle sizes for pristine and 2 M% silver-doped samples are 31.79 nm and 57.60 nm, respectively. The SEM pictures indeed characterize that the particle statures for all the silver doped samples are dissimilar than that for pristine ZnO/CuO composite.

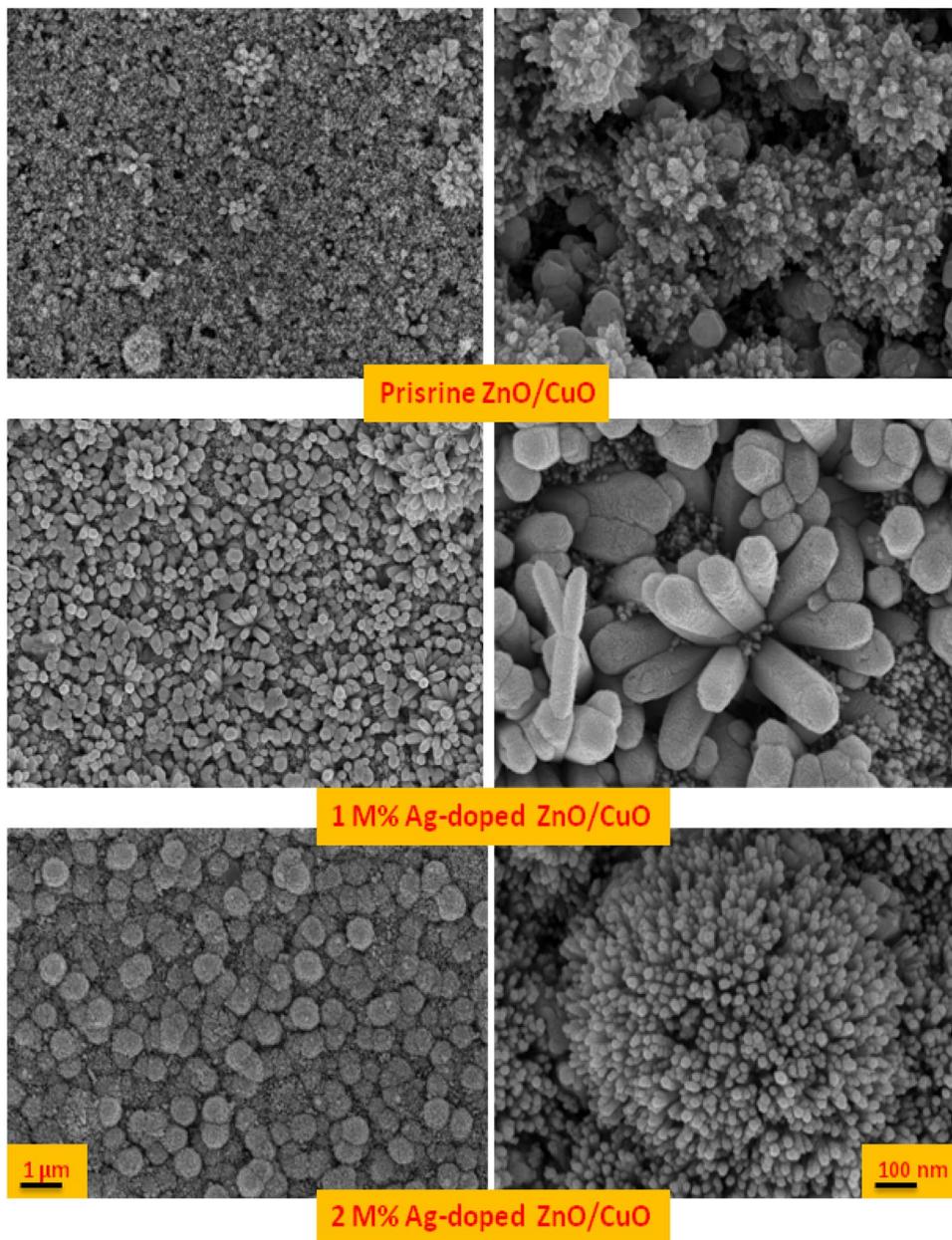
EDX was investigated for the determining of the elemental compositions of grown composite films. Figure 4 presents the EDX spectra of the pristine and silver doped films, which demonstrate the existence of Copper (Cu), Zinc (Zn), Silver (Ag), and Oxygen (O) elements. The atomic percentages of these elements are also tabulated in Table 1.

SEM micrographs have exhibited in the evaluation of the particle distributions. At the same time, AFM was crucial in supplying further knowledge on nanoscale surface properties such as Sa (Average surface roughness), Sq (Root mean square), and Sz (Ten point height). The recorded two and three-dimensional (2D and 3D) AFM micrographs are given in Fig. 5 is with respect to the silver doping content. The changes in the Sa, Sz, and Sq values of grown materials can be related to the differences in the surface structure. Hence, the changes in the particle size influence the surface roughness. The same behavior also observed in earlier reports in the literature [34–36]. The values of the surface roughness parameters like Sa, Sq, and Sz provided from the AFM results are presented as a function of the silver content in Table 2. It can be seen from Table 2, a vigorous decrement in the Sa, Sq, and Sz values appears when the silver percentage is increased from 0 to 2 M%. These findings obtained from the AFM studies are in good agreement with the results of the SEM analysis.

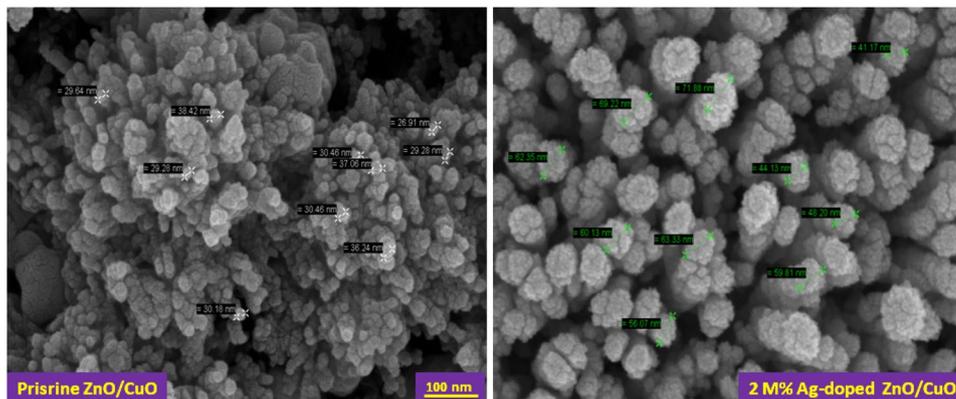
### 3.2 Structural studies of nanostructured ZnO/CuO composite thin films

Crystallographic examinations of ZnO/CuO composite films were conducted using the XRD technique. Figure 6 presents the X-ray spectra of all the ZnO/CuO films at different dopant concentrations. The X-ray diffraction spectrum

**Fig. 2** SEM pictures at  $\times 20,000$  and  $\times 50,000$  magnifications of the nanostructured ZnO/CuO composite thin films SILAR fabricated at different silver doping concentration



**Fig. 3** Extended SEM pictures  $\times 200,000$  magnifications of the nanostructured ZnO/CuO composite thin films SILAR fabricated at different silver doping concentration



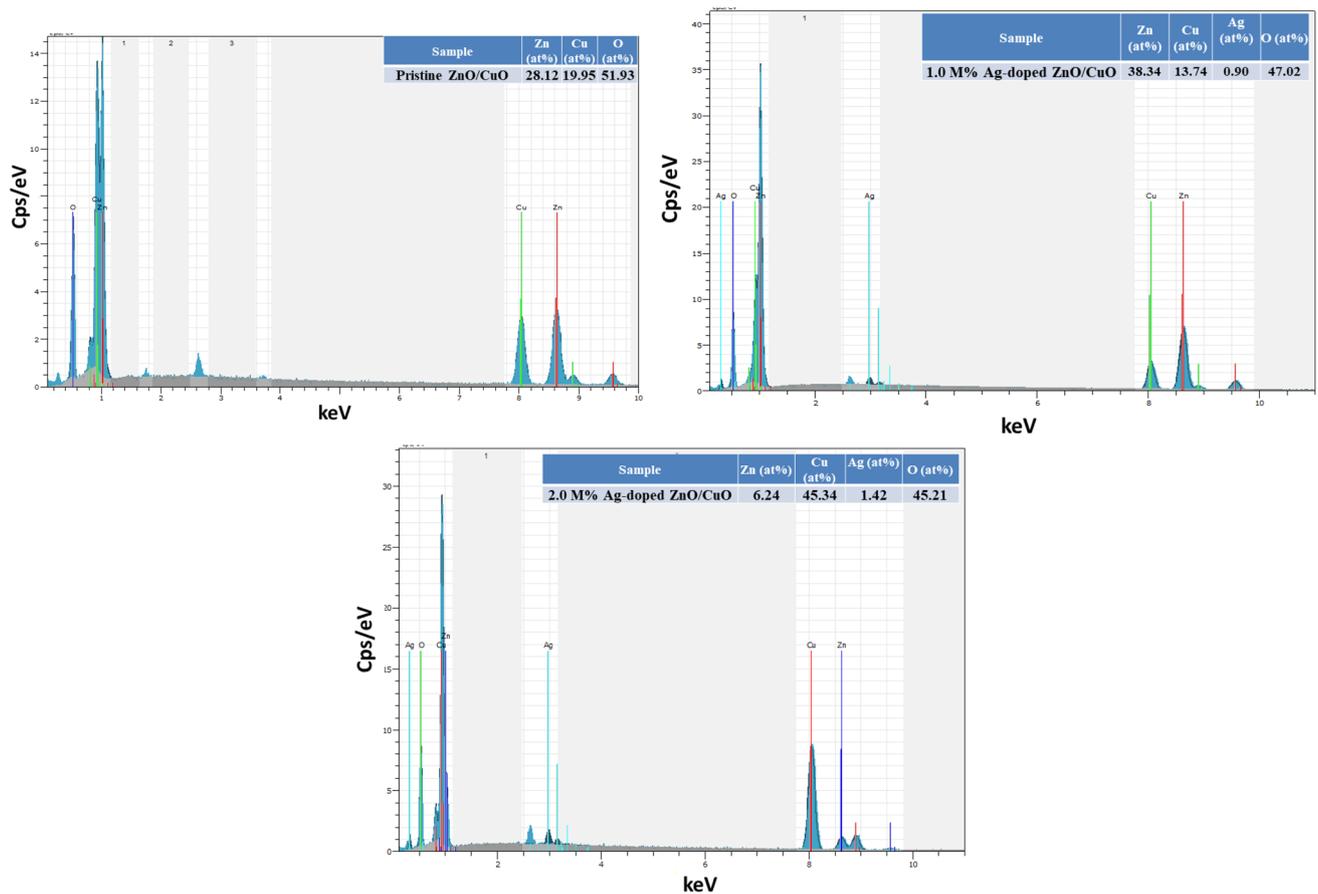


**Fig. 4** Elemental analyses of the nanostructured ZnO/CuO composite thin films SILAR fabricated at different silver doping concentration

**Table 1** Elemental composition of nanostructured ZnO/CuO composite thin films

Sample name	Cu		Zn		O		Ag	
	(at%)	(wt%)	(at%)	(wt%)	(at%)	(wt%)	(at%)	(wt%)
Pristine ZnO/CuO	19.95	32.20	28.12	46.70	51.93	21.10	–	–
1 M% Ag-doped ZnO/CuO	13.74	20.65	38.34	59.27	47.02	17.79	0.90	2.29
2 M% Ag-doped ZnO/CuO	45.34	68.69	6.24	9.73	47.00	17.93	1.42	3.66

showed that all the grown films were polycrystalline in nature. The diffraction peaks were good oriented and well accord with JCPDS card numbers 01-073-8765 and 00-041-0254 for ZnO (hexagonal) and CuO (monoclinic), respectively. The intensities of peaks have detected to be changed with doping percentages. The sharp peak signifies that the obtained thin-film materials have high crystalline quality [37, 38].

There is additionally a shift of  $2\theta$  in (C (002)) diffractions towards lower Bragg angle from 34.49 (for pristine ZnO/CuO) to 34.41 (for 1 M% Ag-doped ZnO/CuO film). This demonstrative change of peak position appears due to the occurred structural strain. The like peak position change was also observed in rare earth element-doped CdO films [39].

Scherrer's equation was used to estimate the crystallite size [40, 41],

$$D = \frac{K\lambda}{\beta \cos \theta} \quad (1)$$

where  $K$  is the Scherrer constant (shape factor) having value 0.94,  $\lambda$  is the wavelength of X-ray,  $\beta$  is the half-height width of the of the diffraction peaks,  $\theta$  is the Bragg's diffraction angle.

The obtained structural parameters are presented in Table 3. The estimated values of the crystallite sizes of the samples were in the range of 16–19 nm as a function of silver content. The slight increase of the crystallite size

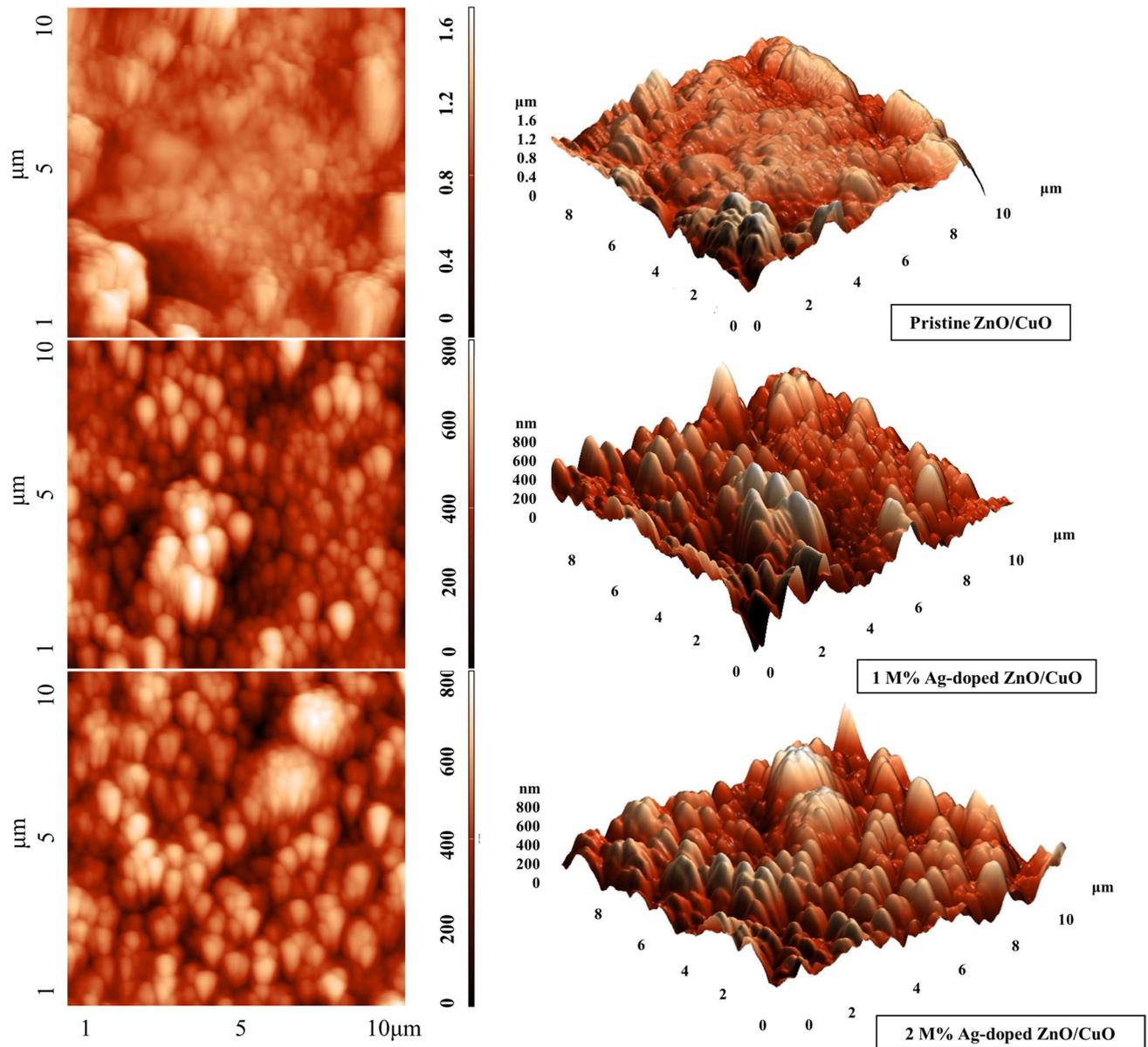


**Fig. 5** 2D and 3D AFM images of the nanostructured ZnO/CuO composite thin films SILAR fabricated at different silver doping concentration over a scan area of  $10\ \mu\text{m} \times 10\ \mu\text{m}$

**Table 2** Main surface roughness parameters of nanostructured ZnO/CuO composite thin films

Sample name	Average surface roughness (Sa) (nm)	RMS (Sq) (nm)	Ten point height (Sz) (nm)	Film thickness ( $\mu\text{m}$ )
Pristine ZnO/CuO	133.82	175.19	852.47	1.79
1 M% Ag-doped ZnO/CuO	103.99	133.00	434.98	1.66
2 M% Ag-doped ZnO/CuO	99.40	123.01	408.78	1.54

for ZnO/CuO film may be described by the substitution of  $\text{Ag}^{2+}$  ions into sites in the ZnO and CuO lattice, which results in distortion of the lattice parameter as reported

in previous studies [42, 43]. This increase in the particle magnitude with silver doping is additionally obtained in the SEM results.

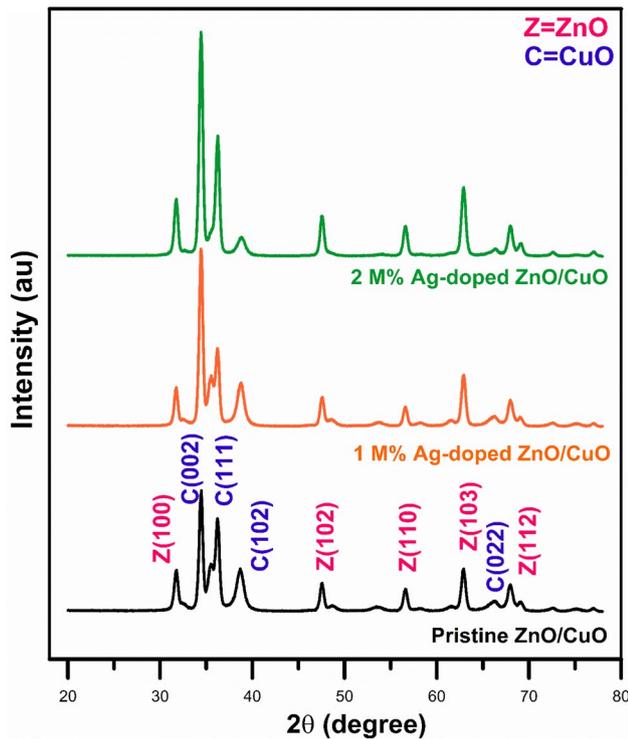


**Fig. 6** X-ray diffraction patterns of the nanostructured ZnO/CuO composite thin films SILAR fabricated at different silver doping concentration

### 3.3 FTIR analysis of nanostructured ZnO/CuO composite thin films

FTIR spectroscopy was used to investigate the various vibrational modes in synthesized particles and the effect of Ag doping. Due to the addition Ag on ZnO/CuO composite, no intense changes were observed in the FTIR spectrum compared to the pristine ZnO/CuO composite sample. This confirmed the conclusion that there is no chemical bond between ZnO/CuO and Ag-based on XRD analysis. Figure 7 shows the FTIR spectrum of the Ag-doped and pristine ZnO/CuO nanocomposite thin films achieved in the range of 500–4000  $\text{cm}^{-1}$ . A few vibration modes were determined in diverse regions of the FTIR spectrum. The absorption peaks at  $\sim 3535\text{--}3810 \text{ cm}^{-1}$  attributed to O–H stretching modes of surface adsorbed water molecules or

hydroxyl groups in M–OH (M=Zn, Cu) [44]. These absorption bands of the composite (OH group) shifted to a higher frequency when Ag content was added to ZnO/CuO nanocomposite thin films, because of the strong hydrogen bond interaction between the composite and metal oxide particles. Also, peaks between the  $2000 \text{ cm}^{-1}$  and  $2930 \text{ cm}^{-1}$  can be attributed to C=O and  $-\text{CH}_2$  vibrations from the residual precursors and organic contaminations [45].

The absorption peak located at  $880 \text{ cm}^{-1}$  was appointed to the characteristic stretching mode of the Zn–O bond [46]. As metal-oxide materials in general exhibit absorption bands in the fingerprint region (i.e., below  $1000 \text{ cm}^{-1}$ ), which arise from inter-atomic vibrations and peaks appearing at  $\sim 725$  to  $\sim 510 \text{ cm}^{-1}$  can be assigned to the metal–oxygen (M–O) (M=Zn, Cu) stretching modes [47].

### 3.4 Optical properties of nanostructured ZnO/CuO composite thin films

The energy bandgap properties of pristine and silver-doped nanostructured ZnO/CuO composite films were determined from the absorbance measurement. The optical bandgap energy ( $E_g$ ) of samples was determined by using the Tauc method [48–50]

$$(\alpha h\nu) = C(h\nu - E_g)^{1/2} \quad (2)$$

where  $C$  is a constant,  $h\nu$  is the photon energy, and  $\alpha$  is the absorption coefficient. The optical bandgap energy of pristine and silver-doped ZnO/CuO composite films was then estimated by extrapolating the linear regions on the energy axis (Fig. 8).

The optical bandgap energy of pristine ZnO/CuO composite film is 2.05 eV. The calculated energy gaps have an excellent accord with the reported from other researcher groups for ZnO/CuO composite films prepared with different techniques [51, 52]. The bandgap energy was increased from 2.05 to 2.36 eV as the Ag content in the growth solution was increased from 0 to 2 M%. These values are also tabulated in Table 3. This result evidently exhibits that the change of the visible-light transmission is based on the presence of silver elements that contributes to the broadening of the bandgap of nanostructured ZnO/CuO composite materials. This is predicated to the influence of the entity of silver ions in the

**Table 3** Relative peak intensity, crystallite size and band gap values of nanostructured ZnO/CuO composite thin films

Sample name	Relative peak intensity (cps) C (002)	Crystallite size (nm)	Bandgap (eV)
Pristine ZnO/CuO	8184	16	$2.05 \pm 0.05$
1 M% Ag-doped ZnO/CuO ZnO/CuO	15942	19	$2.19 \pm 0.05$
2 M% Ag-doped ZnO/CuO	12320	17	$2.36 \pm 0.05$

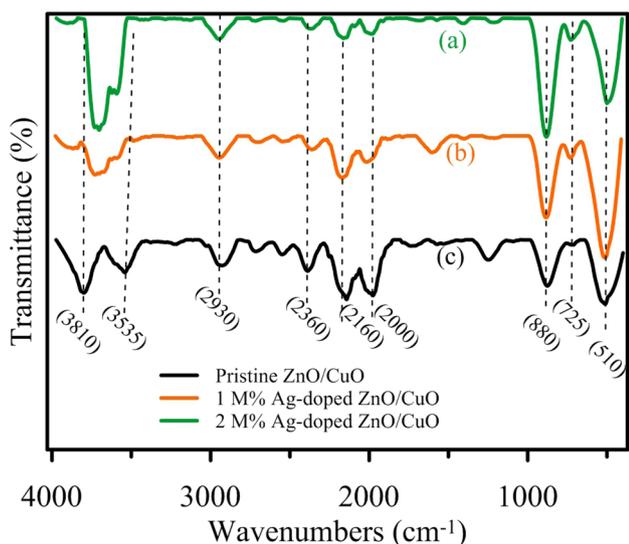


**Fig. 7** FTIR spectroscopy of the nanostructured ZnO/CuO composite thin films SILAR fabricated at different silver doping concentration

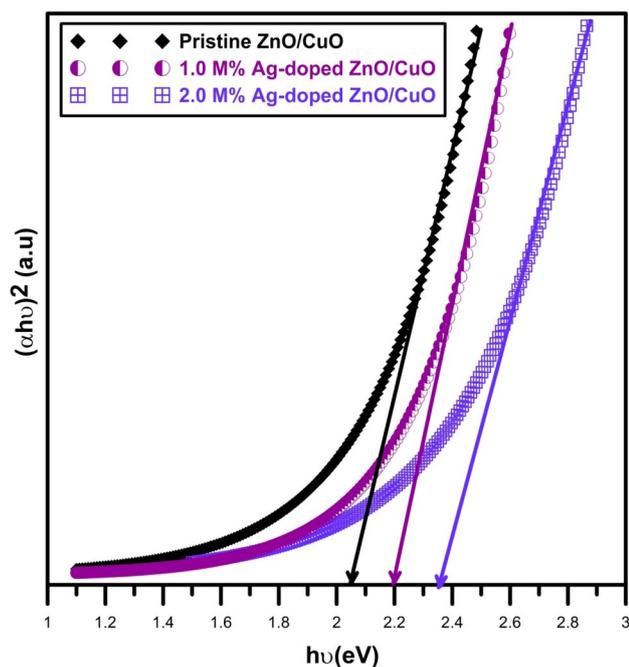


**Fig. 8** Comparison of  $(\alpha h\nu)^2$  versus  $h\nu$  plots of the nanostructured ZnO/CuO composite thin films SILAR fabricated at different silver doping concentration

ZnO/CuO structure to bridge the bandgap energy of pristine ZnO/CuO composite [53].

Meanwhile, the increment in the bandgap with Ag concentration may be related to the change in the form of the surface morphology, particle size and crystallinity quality of the nanostructured metal-oxide materials [54, 55], which was existent with the previous researches [56].

Accordingly, this is because the *3d* orbital of the Zinc atom is overly deep than the *3d* orbital of Copper. Hence, robust coupling arises between the *d* orbital of the Cu atom and the *p* orbital of the O atom, which effects the direct bandgap [57]. This judgment was supported via SEM, AFM, and XRD results.

Figure 9 presents optical transmittance spectra of the nanostructured ZnO/CuO composite samples as a result of Ag percentage in the wavelength range of 400–1100 nm. Pristine ZnO/CuO composite thin film has weak transmittance of less than nearly 3%. At the same time, compared with the pristine ZnO/CuO composite film, the transmittance is obviously enhanced by the doping of silver with the modulation of film properties. The increase in optical transmittance owing to silver doping may be because of alert surface topography, particle size, film thickness, and free carrier concentrations [58]. In addition, it is clearly seen that transmittance values of the samples are increased with the decreasing of film thickness. The thickness could influence the optical absorption and transmission. The similar increasement with decreasing film thickness was further observed for hausmannite ( $Mn_3O_4$ ) thin films [59].

### 3.5 Electrical properties of nanostructured ZnO/CuO composite thin films

Figure 10 shows the resistivity of the pristine, 1 M%, and 2 M% Ag-doped ZnO/CuO composite samples. When Fig. 10 is viewed, an apparent change can be seen in electrical resistivity with Ag-doping. The resistivity was firstly decreased from 397 to 385  $\Omega$  cm by the addition of 1 M%

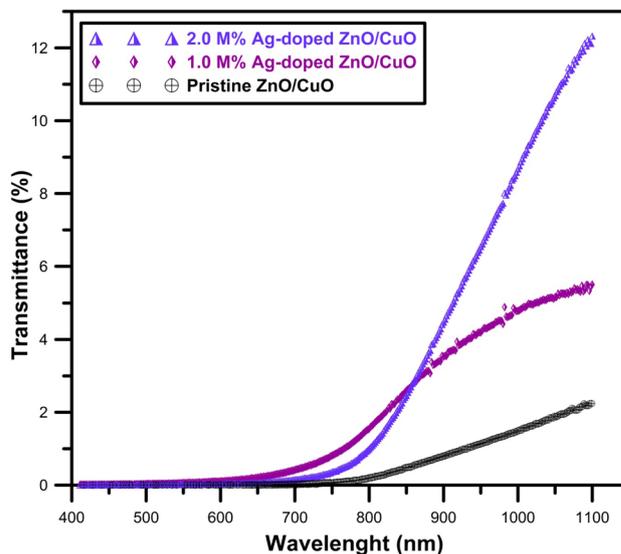


**Fig. 9** Optical transmittance spectra of the nanostructured ZnO/CuO composite thin films SILAR fabricated at different silver doping concentration

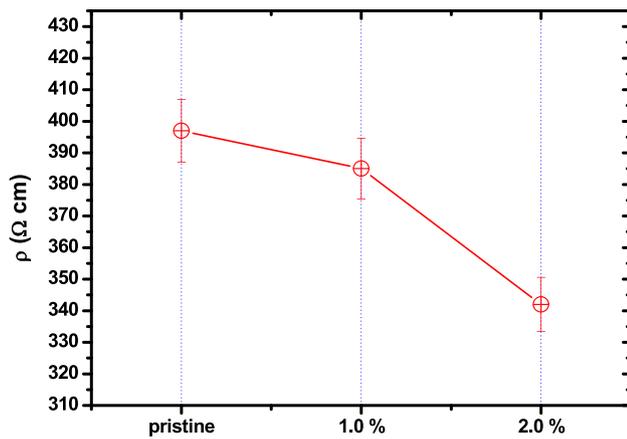


**Fig. 10** Resistivity characteristics of the nanostructured ZnO/CuO composite thin films SILAR fabricated at different silver doping concentration

Ag doping and then from 385 to 342 by 2 M% Ag-doping. As the doping level increased, more dopant atoms reduced resistivity. The decrease in resistivity could be attributed to the doping of new charge carriers to the structure. Afaah et al. prepared Ag-doped ZnO. They observed that a suitable concentration Ag-doping caused an improvement for conductivity [60]. On the other hand, Chiang et al. investigated various metal doping to CuO, including Ag-doping. They reported that Ag-doping decreased resistivity [61]. As can be shown in the literature Ag-doping to both ZnO and CuO reduced resistivity. A similar result was observed in our work that we used ZnO/CuO mixed oxides. The substitution of  $\text{Ag}^{2+}$  ions into sites in the ZnO and CuO lattice leading to an increase of free charge carriers.

Figure 11 shows the Arrhenius plot of  $\ln(\sigma)$  versus  $1/T$  for the pristine, 1 M%, and 2 M% Ag-doped ZnO/CuO composite samples. The electrical conductivity of the samples is described as [62]

$$\sigma = \frac{1}{\rho} \quad (3)$$

where  $\rho$  is a resistivity and Arrhenius equation is defined as

$$\sigma = \sigma_0 e^{\frac{E_a}{kT}} \quad (4)$$

where,  $\sigma_0$  is a pre-exponential factor,  $T$  is the absolute temperature,  $k$  is the Boltzmann constant, and  $E_a$  is the material's activation energy.

When Fig. 11 is viewed, it is seen that the pristine ZnO/CuO mixed oxide has the lowest conductivity at all the temperature region. It is noteworthy that adding 1 M% and 2 M% Ag results in a significant difference in conductivity at all temperature values. This behavior showed us that the doping process was successfully applied due to increasing charge carriers in the samples. In addition, all conductivity

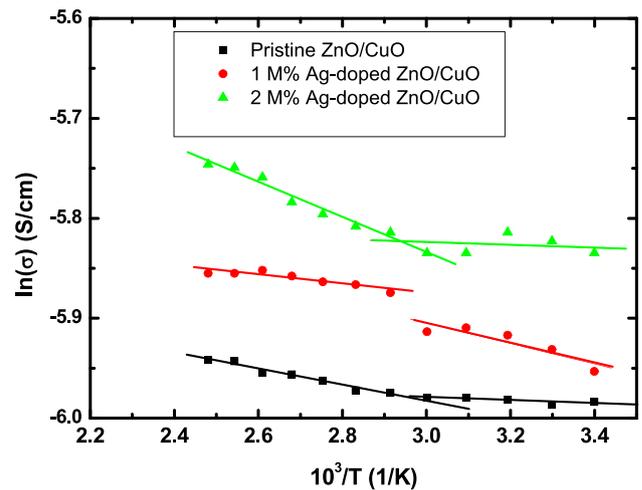


**Fig. 11** Arrhenius plot of  $\ln(\sigma)$  versus  $1/T$  for the nanostructured ZnO/CuO composite thin films SILAR fabricated at different silver doping concentration

curves showed the two-linear regions. This indicates that there is multiple activation process in different temperature regions. A similar attitude can be attributed to a system consisting of an intrinsic semiconductor at high temperature and an extrinsic semiconductor at low temperature [62]. The addition of dopants generates the new mobile carriers at low temperatures in the extrinsic region. Thus, it can be mentioned that there is two activation energy for each sample. The calculated activation energy and pre-exponential factors were tabulated in Table 4. In the table,  $E_{a1}$  and  $\sigma_{o1}$  indicate the activation energy and pre-exponential factor calculated from the high-temperature region of the curves in Fig. 11, while  $E_{a2}$  and  $\sigma_{o2}$  derived from the low-temperature area of the graph. The pre-exponential factor increased with increasing Ag-doping content at the high-temperature region, while no regular change in the other parameters was being observed. 1 M% Ag-doped sample showed different characteristics opposite from the observed doping trend. It can be attributed to crystallite size effects on conductivity [63]. As can be mentioned in Table 3 1 M% Ag-doped sample has the biggest crystallite size parameter.

**Table 4** The calculated activation energy and pre-exponential factor values of nanostructured ZnO/CuO composite thin films

Sample name	$E_{a1}$ (meV)	$E_{a2}$ (meV)	$\sigma_{o1}$ (S/cm)	$\sigma_{o2}$ (S/cm)
Pristine ZnO/CuO	6.66	1.34	$3.19 \times 10^{-3}$	$2.66 \times 10^{-3}$
1 M% Ag-doped ZnO/CuO	4.01	8.79	$3.25 \times 10^{-3}$	$3.71 \times 10^{-3}$
2 M% Ag-doped ZnO/CuO	15.17	1.16	$4.97 \times 10^{-3}$	$3.01 \times 10^{-3}$

## 4 Conclusion

ZnO/CuO composite thin films formed from n-type ZnO and p-type CuO materials were grown by the SILAR technique, and they were analyzed as a function of the Ag doping concentrations. If the analysis results were sorted as structural, surface, optical and electrical; ZnO/CuO composite thin film had a polycrystalline nature with hexagonal-ZnO and monoclinic-CuO structures according to the XRD analysis. FTIR spectra confirmed the Zn–O and Cu–O vibration bands. SEM and AFM results showed that increased Ag doping reduces thin-film porosity. Also, the crystallite size was found to increase from 16 to 19 nm with Ag doping. The bandgap measurements revealed that the bandgap of ZnO/CuO thin film was increased with an increasing Ag doping amount. Also, it was observed that a successful adjustment in the electrical conductivity with Ag doping was possible. Increasing Ag doping caused a decrease in resistivity of ZnO/CuO thin films.

## References

- A.A. Ziabari, F.E. Ghodsi, *J. Alloys Compd.* **509**, 8748 (2011)
- J.K. Rajput, T.K. Pathak, V. Kumar, H.C. Swart, L.P. Purohit, *AIP Conf. Proc.* **1942**, 080035 (2018)
- Ö. Güler, S.H. Güler, Ö. Başgöz, M.G. Albayrak, I.S. Yahia, *Mater. Res. Express* **6**, 095602 (2019)
- M. Sabet, M. Salavati-Niasari, O. Amiri, *Electrochim. Acta* **117**, 504 (2014)
- B. Behera, S. Chandra, *Sens. Actuators B* **229**, 414 (2016)
- T.K. Pathak, J.K. Rajput, V. Kumar, L.P. Purohit, H.C. Swart, R.E. Kroon, *J. Colloid Interface Sci.* **487**, 378 (2017)
- A.M. Ali, O. Qreshah, A.A. Ismail, F.A. Harraz, H. Algarni, M.A. Assiri, M. Faisal, W.S. Chiu, *Int. J. Electrochem. Sci.* **14**, 1461 (2019)
- C. Stella, N. Soundararajan, K. Ramachandran, *Adv. Mater. Lett.* **7**, 652 (2016)
- S.H. Güler, Ö. Güler, E. Evin, S. Islak, *Optik* **127**, 3187 (2016)
- X. Deng, L. Zhang, J. Guo, Q. Chen, J. Ma, *Mater. Res. Bull.* **90**, 170 (2017)
- Y. Orooji, R. Mohassel, O. Amiri, A. Sobhani, M. Salavati-Niasari, *J. Alloys Compd.* **835**, 155240 (2020)
- N. Preda, A. Costas, M. Enculescu, I. Enculescu, *Mater. Chem. Phys.* **240**, 122205 (2020)
- Y. Çağlar, D.D. Oral, M. Çağlar, S. Ilcan, M.A. Thomas, K. Wu, Z. Sun, J. Cui, *Thin Solid Films* **520**, 6642 (2012)
- B. Zhao, F. Mattelaer, J. Kint, A. Werbrouck, L. Henderick, M. Minjauw, J. Dendooven, C. Detavernier, *Electrochim. Acta* **320**, 134604 (2019)
- P. Mehdizadeh, Y. Orooji, O. Amiri, M. Salavati-Niasari, H. Moayedi, *J. Clean. Prod.* **252**, 119765 (2020)
- M. Ramya, T.K. Nideep, K.R. Vijesh, V.P.N. Nampoori, M. Kailasnath, *Opt. Mater.* **81**, 30 (2018)
- B. Şahin, T. Kaya, *Microelectron. Eng.* **164**, 88 (2016)
- M.S. AlSalhi, A. Sakthisabarimoorathi, S. Devanesan, S.A. Martin Britto Dhas, M. Jose, *J. Mater. Sci-Mater. El.* **30**, 13708 (2019)
- W. Fang, L. Yu, L. Xu, *Beilstein J. Nanotechnol.* **11**, 631 (2020)
- M. Poloju, N. Jayababu, M.V. Ramana Reddy, *Mater. Sci. Eng. B* **227**, 61 (2018)
- A.S. Lozhkomoiev, O.V. Bakina, A.V. Pervikov, S.O. Kazantsev, E.A. Glazkova, *J. Mater. Sci-Mater. El.* **30**, 13209 (2019)
- S.E. Elhadi, C. Liu, Y. Guo, K. Li, *J. Alloys Compd.* **785**, 798 (2019)
- F.M. Ali, R.M. Kershi, M.A. Sayed, Y.M. AbouDeif, *Phys. B* **538**, 160 (2018)
- H. Elhosiny Ali, Y. Khairy, H. Algarni, H.I. Elsaedy, A.M. Alshehri, I.S. Yahia, *J. Mater. Sci-Mater. El.* **29**, 20424 (2018)
- H.I. Elsaedy, H.E. Ali, H. Algarni, I.S. Yahia, *Appl. Phys. A* **125**, 79 (2019)
- E.T. Salim, H.T. Halboos, *Mater. Res. Express* **6**, 066401 (2019)
- Y.-Y. Wang, B.-J. Li, L.-J. Huang, H.-D. Cao, L. Zhao, N.-F. Ren, *J. Alloys Compd.* **829**, 154504 (2020)
- M.A. Liaqat, Z. Hussain, Z. Khan, M.A. Akram, A. Shuja, *J. Mater. Sci-Mater. El.* **31**, 7172 (2020)
- Q. Xu, S. Cheng, X. Hao, Z. Wang, N. Ma, P. Du, *Appl. Phys. A* **123**, 289 (2017)
- C.J. Diliiegros-Godines, J. Santos Cruz, N.R. Mathews, M. Pal, *J. Mater. Sci.* **53**, 11562 (2018)
- S.H. Güler, M. Boyrazlı, Ö. Başgöz, F. Yakuphanoglu, *Phys. B* **547**, 120 (2018)
- A. Jamal Sisi, M. Fathinia, A. Khataee, Y. Orooji, *J. Mol. Liq.* **308**, 113018 (2020)
- F. Davar, M. Salavati-Niasari, N. Mir, K. Saberyan, M. Monemzadeh, E. Ahmadi, *Polyhedron* **29**, 1747 (2010)
- Y.S. Ocak, D. Batibay, S. Baturay, *J. Mater. Sci-Mater. El.* **29**, 17425 (2018)
- I. Sta, M. Jlassi, M. Hajji, H. Ezzaouia, *Thin Solid Films* **555**, 131 (2014)
- M. Shirazi, R. Sabet Dariani, M.R. Toroghinejad, *J. Mater. Sci-Mater. El.* **27**, 10226 (2016)
- V.V. Ganbavle, S.V. Mohite, G.L. Agawane, J.H. Kim, K.Y. Rajpure, *J. Colloid Interface Sci.* **451**, 245 (2015)
- E. Yücel, *Superlattice Microstrcut.* **135**, 106287 (2019)
- A.A. Dakhel, *Curr. Appl. Phys.* **11**, 11 (2011)
- S. Goel, N. Sinha, H. Yadav, A.J. Joseph, B. Kumar, *J. Mater. Sci-Mater. El.* **29**, 13818 (2018)
- P.K. Singh, N. Singh, M. Singh, S.K. Singh, P. Tandon, *Appl. Phys. A* **126**, 321 (2020)
- T. Coman, E.L. Ursu, V. Nica, V. Tiron, M. Olaru, C. Cotofana, M. Dobromir, A. Coroaba, O.-G. Dragos, N. Lupu, O.F. Caltun, C. Ursu, *Thin Solid Films* **571**, 198 (2014)
- G. Kaur, A. Mitra, K.L. Yadav, *Prog. Nat. Sci.-Mater.* **25**, 12 (2015)
- D.H. Piva, R.H. Piva, M.C. Rocha, J.A. Dias, O.R.K. Montedo, I. Malavazi, M.R. Morelli, *Adv. Powder Technol.* **28**, 463 (2017)
- Z.R. Khan, M.S. Khan, M. Zulfeqar, M.S. Khan, *Mater. Sci. Appl.* **2**, 340 (2011)
- N. Rao, M. Rao, *Am. J. Mater. Sci.* **5**, 66 (2015)
- S.A. Khan, F. Noreen, S. Kanwal, A. Iqbal, G. Hussain, *Mater. Sci. Eng.: C* **82**, 46 (2018)
- J. Tauc, *Amorphous and Liquid Semiconductors* (Plenum Press, New York, 1974)
- J. Tauc, R. Grigorovici, A. Vancu, *Phys. Status Solidi B* **15**, 627 (1966)
- R. Aydın, B. Şahin, *J. Alloys Compd.* **705**, 9 (2017)
- Y. Yulizar, R. Bakri, D.O.B. Apriandanu, T. Hidayat, *Nano-Struct. Nano-Objects* **16**, 300 (2018)
- N. Widiarti, J. Sae, S. Wahyuni, *IOP Conf. Ser-Mater. Sci.* **172**, 012036 (2017)
- M.A. Hameed, O.A. Ali, S.S.M. Al-Awadi, *Optik* **206**, 164352 (2020)
- E. Gürbüz, R. Aydın, B. Şahin, *J. Mater. Sci-Mater. El.* **29**, 1823 (2018)

55. R. Aydın, B. Şahin, *Ceram. Int.* **43**, 9285 (2017)
56. A. Majid, Z. Afzal, S. Murtaza, G. Nabi, N. Ahmad, *J. Adv. Phys.* **2**, 116 (2013)
57. S. Das, V.C. Srivastava, *Nanotechnol. Rev.* **7**, 267 (2018)
58. C.-H. Zhai, R.-J. Zhang, X. Chen, Y.-X. Zheng, S.-Y. Wang, J. Liu, N. Dai, L.-Y. Chen, *Nanoscale Res. Lett.* **11**, 407 (2016)
59. B. Şahin, B. Aslan, T. Kaya, *Mater. Sci. Semicon. Process.* **98**, 1 (2019)
60. A.N. Afaah, N.A.M. Asib, A. Aadila, R. Mohamed, M. Rusop, Z. Khusaimi, *AIP Conf. Proc.* **1733**, 020055 (2016)
61. C.-Y. Chiang, Y. Shin, S. Ehrman, *Appl. Energy* **164**, 1039 (2016)
62. A.R. West, *Solid State Chemistry and Its Applications* (Wiley, New York, 1984)
63. R.B. Vasiliev, M.N. Rumyantseva, S.G. Dorofeev, Y.M. Potashnikova, L.I. Ryabova, A.M. Gaskov, *Mendeleev Commun.* **14**, 167 (2004)

**Publisher's Note** Springer Nature remains neutral with regard to jurisdictional claims in published maps and institutional affiliations.